



UNIVERSITÀ DEGLI STUDI DI MILANO

Facoltà di Scienze e Tecnologie
Laurea Triennale in Fisica

Simulated run in the rain

Relatore: Prof. Nicola Manini

Cristian Angelo Crespi
Matricola n° 964503
A.A. 2023/2024

Codice PACS: 92.60.jf

Simulated run in the rain

Cristian Angelo Crespi

Dipartimento di Fisica, Università degli Studi di Milano,
Via Celoria 16, 20133 Milano, Italia

Farawember 33, 2399

Abstract

The optimal velocity of running in the rain has long been discussed in the physics and mathematics community, although in practice the human body has always been represented as a simple shape such as a parallelepiped or a cylinder. In this work we use numerical simulations to find results for more complex and dynamical shapes that can represent the human body with an accuracy never reached before in this field.

Advisor: *Prof. Nicola Manini*

Contents

1	Introduction	3
2	The model	4
2.1	Analytic results	6
2.2	The sphere	7
2.3	The parallelepiped	7
2.4	The capsule	8
2.5	The body	10
3	Technical implementation	14
3.1	Code validation	14
4	Results	20
5	Discussion and Conclusion	21
	References	22

1 Introduction

The question of whether it is better to run or walk in the rain is as old as time, and has proven to be a recurring topic in the mathematics and physics community in the last 50 years. Despite the relatively few articles on the topic and the large time span in which they have been produced there have been precious little improvements upon the results first found by Schwartz and Deakin [1] back in 1973. In that article an orthogonal parallelepiped (from here on we will refer to orthogonal parallelepipeds simply as parallelepipeds as done in previous works on the topic) with sides parallel to the axes is used to approximate a human body running on a straight path in the presence of rain and wind, leading the following results: in the presence of a strong enough tailwind an ideal speed exists, and it equals the component of the rain velocity along the direction of the path; without a tailwind it is always er to run faster, although with diminishing returns. Since then a variety of simple geometric shapes have been considered: spheres [2, 3], cylinders [3], paraboloids [2], plane surfaces [3] and parallelepipeds with generic orientations [3]. What we can see is that the shape considered can change the results considerably: in the presence of a strong enough tailwind a finite ideal speed always exists, but its value depends on the shape considered, and for some shapes an ideal speed can exist even without wind or in the presence of headwind. Because of these discordant results the need for a better approximation of the human body becomes apparent, and the only reason this has not been done yet is the difficulty of deriving analytical results for complex shapes. In the present work we will address this problem by means of a numerical approach. A numerical approach to the problem has been already tried [4], but it too only modeled the human body as a parallelepiped, and its focus was instead on comparing modeling rain as raindrops placed in a cubic lattice as opposed to the more realistic case in which the raindrops are generated at random positions; as expected, the two models agree well.

In this work we consider a model of the body consisting of multiple elementary three-dimensional geometric shapes that move relative to each other, which we will refer to as body parts. We used  spheres, parallelepipeds and capsules to model individual body parts. A capsule, also sometimes called a spherocylinder, is an elementary three-dimensional shape consisting in a cylinder with hemispherical ends. Capsules had never been studied before in this context so we had to derive an explicit analytical solution.

2 The model

We model a person running along a straight path under rain and wind. We want to determine is the ideal speed at which she/he should move such that she/he catches the least possible amount of rain. We shall assume the following:

1. The ground is horizontal.
2. The path is rectilinear.
3. The raindrops all have the same size and are densely and uniformly distributed in space.
4. The wind velocity is constant and the raindrops have reached their terminal velocity in the wind.
5. The wind adds a horizontal component to the velocity of the rain.
6. The motion of the body consists of a translation at constant speed along the path plus a periodic relative motion that is generally unique to each body part but shares the same period T .
7. The velocity of the body parts due to their periodic motion is negligible compared to the velocity of the rain.
8. The path is long enough that periods of the periodic motions of the body parts are small compared to the time t_f taken to traverse the path ($T \ll t_f$).
9. All involved speeds are negligible compared to the speed of light, so that the nonrelativistic limit and Galilean transformations apply throughout.

In the rest frames of reference, the x axis is aligned with the path of the body and the z axis is be the vertical axis. According to assumptions 1, 2 and 6 the body is translating with a velocity $\mathbf{v}_b = v_b \hat{\mathbf{e}}_x$, and the rain has a velocity \mathbf{v}_r . The z component of \mathbf{v}_r is negative, and we refer to its absolute value as the falling velocity v_{fall} . We refer to the value of the y component of \mathbf{v}_r as the "crosswind" v_{cross} . We refer to the value of the x component of \mathbf{v}_r as the "tailwind" v_{tail} if it is positive and to its absolute value as the "headwind" v_{head} if it is negative. We call $d = v_b t_f$ the total length of the path traversed.

The wetness W of the traveler, measured as the total volume of water that has hit her/him at the end of the walk, is equal to the number of raindrops hit times the volume of each drop. Thanks to our assumption 3 we can safely define a dimensionless "rain density" $\rho_{rain} = N_{drop} V_{drop} / V$, where N_{drop} is the number of raindrops contained in

a certain volume V and V_{drop} is the volume of a single drop. In short ρ_{rain} is the ratio between the amount of rain contained in a volume and that same volume, i.e. the volume fraction of liquid water freely falling in the atmosphere. Let us consider the frame of reference in which the raindrops are still. In this frame the velocity of the body is \mathbf{v}_{rel} – \mathbf{v}_b . The stationary raindrops inside the volume of space that our body passes through, which we call V_b , are swept up by the body motion and contribute to its wetness W . We can then use the following relation to evaluate the wetness: $W = \rho_{rain} V_b$. Since ρ_{rain} is constant in the walk in the rain our problem reduces to evaluating and minimizing V_b . As found in [2] for a body whose only movement is a rigid translation V_b is given by the following formula:

$$V_b(\mathbf{v}_{rel}) = S_b(\mathbf{v}_{rel}) \frac{\|\mathbf{v}_{rel}\|}{v_b} d. \quad (1)$$

$S_b(\mathbf{v}_{rel})$ is the area of the projection of the body on a plane perpendicular to \mathbf{v}_{rel} . The only non-trivial part of the problem is then the determination of the dependence of S_b on \mathbf{v}_{rel} . Note that generally $\lim_{v_b \rightarrow +\infty} V_b(\mathbf{v}_{rel}) \neq 0$; as v_b approaches infinity, \mathbf{v}_{rel} approaches $v_b \hat{\mathbf{e}}_x$, so we get:

$$\lim_{v_b \rightarrow +\infty} V_b(\mathbf{v}_{rel}) = S_b(\hat{\mathbf{e}}_x) d. \quad (2)$$

This shows that even if there is no finite ideal speed there is a minimum wetness that is not avoidable by going faster, which is independent of the rain velocity v_r . Furthermore $\lim_{v_b \rightarrow 0^+} S_b(\mathbf{v}_{rel})$ (which is a reasonable assumption for a human body) then $V_b(\mathbf{v}_{rel})$ diverges to infinity as v_b tends to 0 because of the v_b term in the denominator so there usually is no upper limit to the wetness.

We now generalize these findings for a dynamical body. Since the velocity of the body parts is small compared to the velocity of the rain 7 we can approximate the relative velocity of the body parts with the relative velocity of the whole body \mathbf{v}_{rel} . This way we can write the area of the projection of the whole body as depending only on the relative velocity of the whole body and of the instant orientation of each body part, which only depend on time for a set body: $\tilde{S}_b(\mathbf{v}_{rel}, t)$. We can then generalize Eq.(1) by considering that $d/v_b = t_f$ and substituting $S_b(\mathbf{v}_{rel}) t_f$ with an integral of $\tilde{S}_b(\mathbf{v}_{rel}, t)$ over $[0, t_f]$:

$$V_b = \|\mathbf{v}_{rel}\| \int_0^{t_f} dt \tilde{S}_b(\mathbf{v}_{rel}, t). \quad (3)$$

Furthermore since the time spent traversing the path is long compared to the period of the function $\tilde{S}_b(\mathbf{v}_{rel}, t)$ we can approximate it with its time average over the period T . For a dynamic body we can then employ the time average

$$S_b(\mathbf{v}_{rel}) = \frac{1}{T} \int_0^T dt \tilde{S}_b(\mathbf{v}_{rel}, t) \quad (4)$$

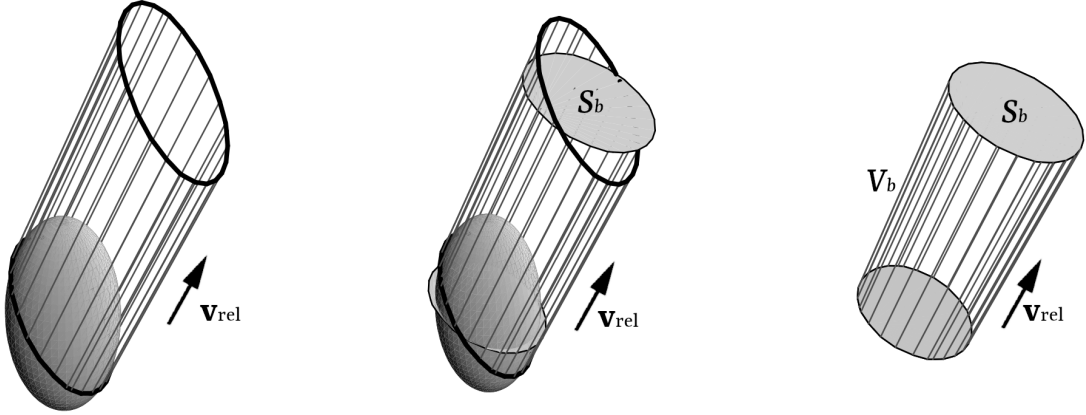


Figure 1: Example with an ellipsoid as the body. Its orthogonal projection on the plane perpendicular to \mathbf{v}_{rel} is a disk with area S_b and V_b is the volume of the resulting cylinder. Original image from [2].

in Eq. (3), which is thus extended to dynamical bodies too, provided that assumptions 6, 7, and 8 are satisfied.

Note that the results are invariant under the transformation $\mathbf{v}_{rel} \rightarrow -\mathbf{v}_{rel}$, since a plane perpendicular to \mathbf{v}_{rel} is also perpendicular to $-\mathbf{v}_{rel}$. Since we won't be able to solve the dynamic body analytically we will approximate $S_b(\mathbf{v}_{rel})$ with a discrete time average:

$$S_b(\mathbf{v}_{rel}) \approx \frac{1}{N} \sum_{i=0}^{N-1} \tilde{S}_b \left(\mathbf{v}_{rel}, i \frac{T}{N} \right). \quad (5)$$

Furthermore, since d is constant we will evaluate and minimize the ratio of wetting volume to path length instead, which can be written as:

$$R_b(\mathbf{v}_{rel}) = \frac{V_b(\mathbf{v}_{rel})}{d} = S_b(\mathbf{v}_{rel}) \frac{\|\mathbf{v}_{rel}\|}{v_b}. \quad (6)$$

For the sake of convenience we will use v_{fall} as a unit of measure for $\mathbf{v}_{rel}, v_b, v_{head}, v_{tail}$ and v_{cross} . We do this since R_b is invariant under the transformation $v_b \rightarrow k v_b$, $\mathbf{v}_{rel} \rightarrow k \mathbf{v}_{rel}$, with $k > 0$. As we can see from Eq. (6), R_b has the dimensions of an area and will thus be measured in m^2 .

2.1 Analytic results

The elementary geometric shapes we adopt as building blocks for a body are spheres, parallelepipeds and capsules. To check if our numerical code works properly it is useful to support the analytic solutions. Furthermore, we need to derive the appropriate formulas

for the projection of ~~the~~ bodies onto planes. First we define the orthogonal projection onto planes perpendicular to a generic vector \mathbf{v} . For simplicity's sake we consider planes passing through the origin. The projector operator $P_{\mathbf{v}}$ onto a plane through the origin and perpendicular to \mathbf{v} can be written as [6]:

$$P_{\mathbf{v}}(\mathbf{a}) = \mathbf{a} - \frac{\mathbf{a} \cdot \mathbf{v}}{\mathbf{v} \cdot \mathbf{v}} \mathbf{v}. \quad (7)$$

Considering bodies B defined as sets of points in \mathbb{R}^3 we define their projection as $P_{\mathbf{v}}(B) := \{P_{\mathbf{v}}(\mathbf{b}) : \mathbf{b} \in B\}$.

2.2 The sphere

The sphere is the easiest body to work with since its projection does not depend on ~~v_{rel}~~ . the orthogonal projection of a sphere of radius r and center \mathbf{c} on any plane is a disk with radius r and center $P_{\mathbf{v}}(\mathbf{c})$ [2][3]. Obviously, its area is, $S_s = \pi r^2$. Plugging this result into Eq. (6), we obtain the following formula for $R_s(\mathbf{v}_{rel})$:

$$R_s(\mathbf{v}_{rel}) = \pi r^2 \frac{\|\mathbf{v}_{rel}\|}{v_b}. \quad (8)$$

Using ~~$\mathbf{v}_{rel} = \mathbf{v}_r - \mathbf{v}_b$~~ and $\mathbf{v}_b = v_b \hat{\mathbf{e}}_x$ we can write $R_s(v_b)$ for any given \mathbf{v}_r :

$$R_s(v_b) = \pi r^2 \frac{\|(\mathbf{v}_r - v_b \hat{\mathbf{e}}_x)\|}{v_b}. \quad (9)$$

And as $v_b \rightarrow +\infty$ we get:

$$\lim_{v_b \rightarrow +\infty} R_s(v_b) = \pi r^2. \quad (10)$$

2.3 The parallelepiped

As found in [1, 2, 3, 4], when dealing with a parallelepiped one only needs to consider the faces that get wet, which are one to three depending on orientations of the parallelepiped and of \mathbf{v} . A parallelepiped is defined by its center \mathbf{c} and its three sides $\mathbf{s}_1, \mathbf{s}_2$ and \mathbf{s}_3 , where $\mathbf{s}_i \cdot \mathbf{s}_j = 0$ for $i, j = 1, 2, 3$ and $i \neq j$. The 6 points corresponding to the centers of its 6 faces are $\mathbf{p}_i^\pm = \mathbf{c} \pm \mathbf{s}_i/2$. We consider the surface of a face as pointing out of the parallelepiped. Then the face with center \mathbf{p}_i^\pm will have surface $\mathbf{S}_i^\pm = \pm \|\mathbf{s}_j \times \mathbf{s}_k\| \hat{\mathbf{s}}_i$, with $\hat{\mathbf{s}}_i = \mathbf{s}_i / \|\mathbf{s}_i\|$ and i, j, k all different. In the system of reference in which the rain is still, the parallelepiped translates with velocity \mathbf{v}_{rel} , and it is easy to see that a face \mathbf{S}_i^\pm gets wet if and only if the velocity of the body is positive in the direction the face is pointing to, i.e. iff $\mathbf{S}_i^\pm \cdot \mathbf{v}_{rel} > 0$, which is equivalent to $\pm \mathbf{s}_i \cdot \mathbf{v}_{rel} > 0$. We can immediately see that if \mathbf{S}_i^\pm gets wet then \mathbf{S}_i^\mp does not, and iff $\mathbf{s}_i \cdot \mathbf{v}_{rel} = 0$ neither of them gets wet, so at most 3 faces can get wet. Since \mathbf{s}_i are 3 orthogonal vectors, they form a complete basis of \mathbb{R}^3 , and since \mathbf{v}_{rel} is never a null vector, then $\mathbf{s}_i \cdot \mathbf{v}_{rel} \neq 0$ for at least one i .

We now want to evaluate the projections of the wet faces on a plane perpendicular to \mathbf{v}_{rel} . The projection of a face is a parallelogram with as vertices the projections of the vertices of the face, and then as sides the projections of the sides of the face. The area of said parallelogram is:

$$A_i(\mathbf{v}_{rel}) = \|(\mathbf{s}_j \times \mathbf{s}_k) \cdot \hat{\mathbf{v}}_{rel}\|, \quad (11)$$

with $\hat{\mathbf{v}}_{rel} = \mathbf{v}_{rel}/\|\mathbf{v}_{rel}\|$. Notice that if we have three wet faces $\mathbf{S}_1, \mathbf{S}_2, \mathbf{S}_3$ each has two sides in common with the others and they all share the vertex connecting the shared sides. The projection of those three faces will then be made up of three parallelograms that each share two sides and a vertex as the original faces. This results in an irregular hexagon with an area equal to the sum of the areas of the 3 composing parallelograms. Its area, which corresponds to $S_p(\mathbf{v}_{rel})$ then is:

$$S_p(\mathbf{v}_{rel}) = \|\mathbf{S}_1 \cdot \hat{\mathbf{v}}_{rel}\| + \|\mathbf{S}_2 \cdot \hat{\mathbf{v}}_{rel}\| + \|\mathbf{S}_3 \cdot \hat{\mathbf{v}}_{rel}\|, \quad (12)$$

with $\mathbf{S}_i = \mathbf{s}_j \times \mathbf{s}_k$. This formula holds even if less than three faces get wet since if $\mathbf{s}_i \cdot \mathbf{v}_{rel} = 0$ then $\|(\mathbf{s}_j \times \mathbf{s}_k) \cdot \mathbf{v}_{rel}\| = 0$, indicating that the contribution by faces that do not get wet vanishes. We can then use Eq. (6) find $R_p(\mathbf{v}_{rel})$:

$$R_p(\mathbf{v}_{rel}) = \left[\sum_{i=1}^3 \|\mathbf{S}_i \cdot \mathbf{v}_{rel}\| \right] \frac{\|\mathbf{v}_{rel}\|}{v_b}. \quad (13)$$

Using $\mathbf{v}_{rel} = \mathbf{v}_r - \mathbf{v}_b$ and $\mathbf{v}_b = v_b \hat{\mathbf{e}}_x$ we can write $R_p(v_b)$ for any given \mathbf{v}_r :

$$R_p(v_b) = \left[\sum_{i=1}^3 \|\mathbf{S}_i \cdot (\mathbf{v}_r - v_b \hat{\mathbf{e}}_x)\| \right] \frac{\|\mathbf{v}_r - v_b \hat{\mathbf{e}}_x\|}{v_b}. \quad (14)$$

And as $v_b \rightarrow +\infty$ we get:

$$\lim_{v_b \rightarrow +\infty} R_p(v_b) = \sum_{i=1}^3 \|\mathbf{S}_i \cdot \hat{\mathbf{e}}_x\|. \quad (15)$$

2.4 The capsule

As stated before while spheres and parallelepipeds have already been studied in this context, capsules (see Fig. 2) are a new shape, so we provide here a simple analytical solution. A capsule is defined as follows [5]: let L be a line segment in \mathbb{R}^3 and r a positive real number. The capsule with axis L and radius r is the set of points whose distance from L is smaller or equal to r . The same capsule can also be defined as the Minkowski sum between L and a ball centered at the origin with radius r . Given two sets of vectors \mathbf{A} and \mathbf{B} in Euclidean space, their Minkowski sum is the set of

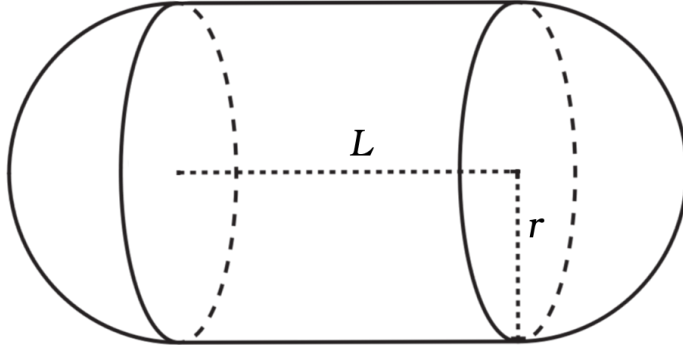


Figure 2: A capsule with axis L and radius r .

points $A + B := \{\mathbf{a} + \mathbf{b} : \mathbf{a} \in A, \mathbf{b} \in B\}$ [7]. We now proceed to find the orthogonal projection of a capsule C on a plane perpendicular to a generic vector \mathbf{v} . We show that $P_{\mathbf{v}}$ distributes over the Minkowski sum, i.e. $P_{\mathbf{v}}(A + B) = P_{\mathbf{v}}(A) + P_{\mathbf{v}}(B)$. Using Eq. (7):

$$P_{\mathbf{v}}(\mathbf{a} + \mathbf{b}) = \mathbf{a} + \mathbf{b} - \frac{(\mathbf{a} + \mathbf{b}) \cdot \mathbf{v}}{\mathbf{v} \cdot \mathbf{v}} \mathbf{v} = \mathbf{a} - \frac{\mathbf{a} \cdot \mathbf{v}}{\mathbf{v} \cdot \mathbf{v}} \mathbf{v} + \mathbf{b} - \frac{\mathbf{b} \cdot \mathbf{v}}{\mathbf{v} \cdot \mathbf{v}} \mathbf{v} = P_{\mathbf{v}}(\mathbf{a}) + P_{\mathbf{v}}(\mathbf{b}), \quad (16)$$

$$\begin{aligned} P_{\mathbf{v}}(A + B) &= \{P_{\mathbf{v}}(\mathbf{a} + \mathbf{b}) : \mathbf{a} \in A, \mathbf{b} \in B\} = \\ &= \{P_{\mathbf{v}}(\mathbf{a}) + P_{\mathbf{v}}(\mathbf{b}) : \mathbf{a} \in A, \mathbf{b} \in B\} = \\ &= \{\mathbf{a}' + \mathbf{b}' : \mathbf{a}' \in P_{\mathbf{v}}(A), \mathbf{b}' \in P_{\mathbf{v}}(B)\} = P_{\mathbf{v}}(A) + P_{\mathbf{v}}(B). \end{aligned} \quad (17)$$

Incidentally, note that while we are only considering vectors in \mathbb{R}^3 and a surface in \mathbb{R}^2 equations 16 and 17 hold up for vectors in \mathbb{E}^n and hypersurfaces in \mathbb{E}^{n-1} for any n . We know that the projection of a line segment L defined by its two endpoints \mathbf{l}_1 and \mathbf{l}_2 is the line segment $\hat{L} = P_{\mathbf{v}}(L)$ with endpoints $P_{\mathbf{v}}(\mathbf{l}_1)$ and $P_{\mathbf{v}}(\mathbf{l}_2)$, and that the projection of a sphere S with radius r centered at the origin is a disk \hat{S} with radius r also centered at the origin and laying on the projection plane. The projection of our capsule $C = L + S$ then is $\hat{C} = \hat{L} + \hat{S}$. The Minkowski sum between a line segment and a disk is the stadium [8], also called sausage body, a two-dimensional geometric shape defined exactly like a capsule, but in 2D. The stadium with axis L and radius r is the set of points whose distance from L is smaller or equal to r . Revolving a stadium around L results in a capsule. An example of a stadium with radius r and axis L can be seen in Fig. 3. The area of a stadium can be easily found considering that it is made up of two half disks with radius r plus a rectangle with sides $2r$ and l , where by l we indicate the length of L , i.e. the Euclidean distance between its two endpoints. The area is:

$$A = \pi r^2 + \underline{r} l. \quad (18)$$

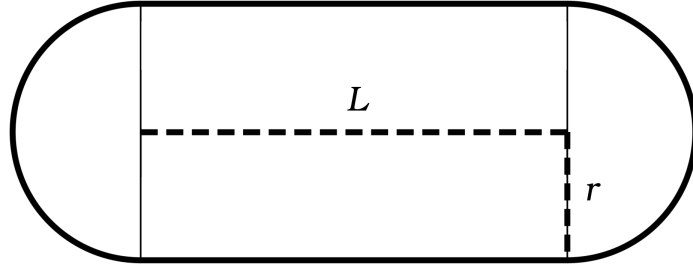


Figure 3: A stadium with radius r and axis L .

The stadium we get from projecting a capsule then has the same radius r , and $\hat{L} = P_{\mathbf{v}}(L)$. Defining $\Delta \mathbf{l} := \mathbf{l}_2 - \mathbf{l}_1$ we can find the length of \hat{L} as:

$$\hat{l} = \|P_{\mathbf{v}}(\mathbf{l}_2) - P_{\mathbf{v}}(\mathbf{l}_1)\| = \|P_{\mathbf{v}}(\Delta \mathbf{l})\| = \left\| \Delta \mathbf{l} - \frac{\Delta \mathbf{l} \cdot \mathbf{v}}{\mathbf{v} \cdot \mathbf{v}} \mathbf{v} \right\|. \quad (19)$$

We now have all we need to calculate the projection S_c of our capsule on a plane perpendicular to the relative velocity of the rain \mathbf{v}_{rel} . Using equations (18) and (19) we write:

$$S_c(\mathbf{v}_{rel}) = \pi r^2 + r \left\| \Delta \mathbf{l} - \frac{\Delta \mathbf{l} \cdot \mathbf{v}_{rel}}{\mathbf{v}_{rel} \cdot \mathbf{v}_{rel}} \mathbf{v}_{rel} \right\|. \quad (20)$$

Substituting Eq. (6) gives us the ratio R_c :

$$R_c(\mathbf{v}_{rel}) = \left[\pi r^2 + r \left\| \Delta \mathbf{l} - \frac{\Delta \mathbf{l} \cdot \mathbf{v}_{rel}}{\mathbf{v}_{rel} \cdot \mathbf{v}_{rel}} \mathbf{v}_{rel} \right\| \right] \frac{\|\mathbf{v}_{rel}\|}{v_b}. \quad (21)$$

Using $\mathbf{v}_{rel} = \mathbf{v}_r - \mathbf{v}_b$ and $\mathbf{v}_b = v_b \hat{\mathbf{e}}_x$ we can write $R_c(v_b)$ for any given \mathbf{v}_r :

$$V_c(v_b) = \left[\pi r^2 + r \left\| \Delta \mathbf{l} - \frac{\Delta \mathbf{l} \cdot (\mathbf{v}_r - v_b \hat{\mathbf{e}}_x)}{(\mathbf{v}_r - v_b \hat{\mathbf{e}}_x) \cdot (\mathbf{v}_r - v_b \hat{\mathbf{e}}_x)} (\mathbf{v}_r - v_b \hat{\mathbf{e}}_x) \right\| \right] \frac{\|(\mathbf{v}_r - v_b \hat{\mathbf{e}}_x)\|}{v_b}. \quad (22)$$

And as $v_b \rightarrow +\infty$ we get:

$$\lim_{v_b \rightarrow +\infty} R_c(v_b) = \pi r^2 + r \left\| \Delta \mathbf{l} - (\Delta \mathbf{l} \cdot \hat{\mathbf{e}}_x) \hat{\mathbf{e}}_x \right\|. \quad (23)$$

2.5 The Body

Considering the wide variety of body types that human beings can exhibit it would seem like an impossible task to find general results for them, and it probably is, so in this work we will limit ourselves to building one specific model of a human body. To make sure that our model can properly approximate a real human we have decided to build it using as a guideline the Vitruvian Man, by Leonardo da Vinci [9]. By analysing

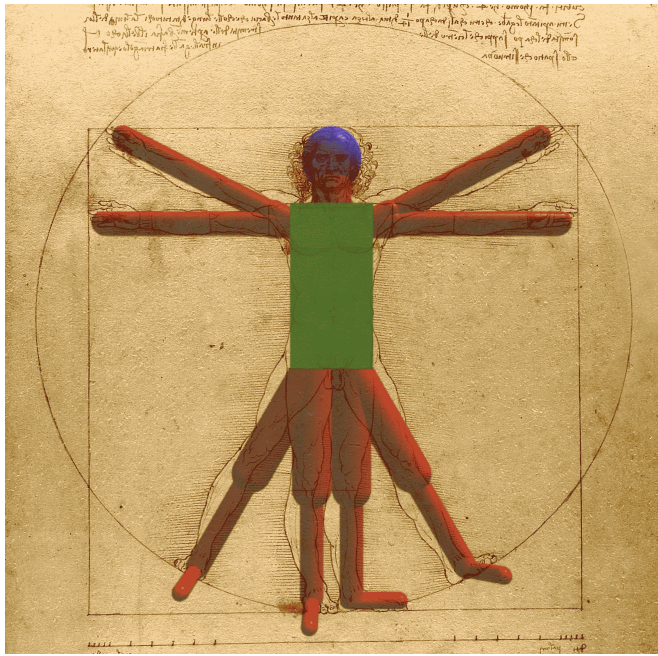


Figure 4: Our model of the human body compared to the Vitruvian Man by Leonardo da Vinci. The colors denote the shape of the body part: blue for spheres, green for parallelepiped and red for capsules.

the text accompanying the drawing and measuring the drawing itself¹ we found the following proportions to follow, given a body with a total height h :

- The head is $h/8$ tall.
- The neck is $h/24$ tall and $h/14$ thick.
- The torso is $h/3$ tall, around $h/6$ wide and around $h/12$ thick.
- The shoulders are each $h/24$ long and around $h \cdot 0.06$ thick.
- The upper arms are each $h/8$ long and around $h/20$ thick.
- The forearms (including the hands) are each $h/4$ long and around $h/20$ thick.
- The thighs are each $h/4$ long and around $h/12$ thick.
- The lower legs are each $h/4$ long and around $h/20$ thick.
- The feet are each $h/7$ long and around $h/30$ thick.

¹We measured a scan of the original drawing using the software ImageJ.

A height of 168 cm was chosen somewhat arbitrarily since it's a multiple of both 8, 3 and 7 and it's a plausible height for a person. Furthermore the velocity should not depend on the size of the body but only on its shape.

As anticipated we built our body using as base shapes spheres, parallelepipeds and capsules. A direct comparison between our model of the body and the Vitruvian Man can be seen in Fig. 4. The numerical details of our body are available on GitHub at <https://github.com/Cr3sp1/RainSimulation/tree/main/Bodies>. Now that we have our body we have to make it move. We chose to study two regimes of motion: walking and running. We decided to model both walking and running with periodic oscillations of the limbs around their respective joints. For simplicity's sake we will approximate the periodic time evolution of the angles θ of the joints as sinusoids:

$$\theta(t) = \frac{\theta_{max} + \theta_{min}}{2} + \frac{\theta_{max} - \theta_{min}}{2} \sin(2\pi t + \phi). \quad (24)$$

To make sure our dynamic body at least resembles a real human being we refer to articles on the biomechanics of walking and running for the amplitudes and relative phases of our sinusoids. Considering for each joint the angle $\theta = 0$ when the body is standing with straight legs and the arms parallel to the body, and $\theta > 0$ when the limb moves forward along the direction of motion of the body:

- During both walking and running the angle of the arm at the shoulder θ_{sho} is in counterphase with the angle of the same side leg at the hip θ_{hip} . During walking θ_{sho} ranges from $\sim -30^\circ$ to $\sim 20^\circ$, while during running θ_{sho} ranges from $\sim -30^\circ$ to $\sim 0^\circ$ [10].
- During both walking and running the angle of the arm at the elbow θ_{elb} is in phase with θ_{sho} . During walking θ_{elb} ranges from $\sim 5^\circ$ to $\sim 25^\circ$, while during running θ_{elb} ranges from $\sim 85^\circ$ to $\sim 110^\circ$ [10].
- During walking θ_{hip} ranges from $\sim -10^\circ$ to $\sim 30^\circ$ [11], while during running θ_{hip} ranges from $\sim -30^\circ$ to $\sim 30^\circ$ [12].
- During both walking and running the angle of the leg at the knee θ_{kne} has a relative phase of around $-\pi/2$ with θ_{hip} . During walking θ_{kne} ranges from $\sim -60^\circ$ to $\sim 0^\circ$ [11], while during running θ_{kne} ranges from $\sim -120^\circ$ to $\sim -15^\circ$ [12].
- During both walking and running the angle of the ankle θ_{ank} is in antiphase with θ_{kne} . During walking θ_{ank} ranges from $\sim -5^\circ$ to $\sim 20^\circ$ [11], while during running θ_{ank} ranges from $\sim -30^\circ$ to $\sim 25^\circ$ [12].
- All the angles formed by limbs on one side of the body are in counterphase with the angles formed by the corresponding limbs on the other side of the body.

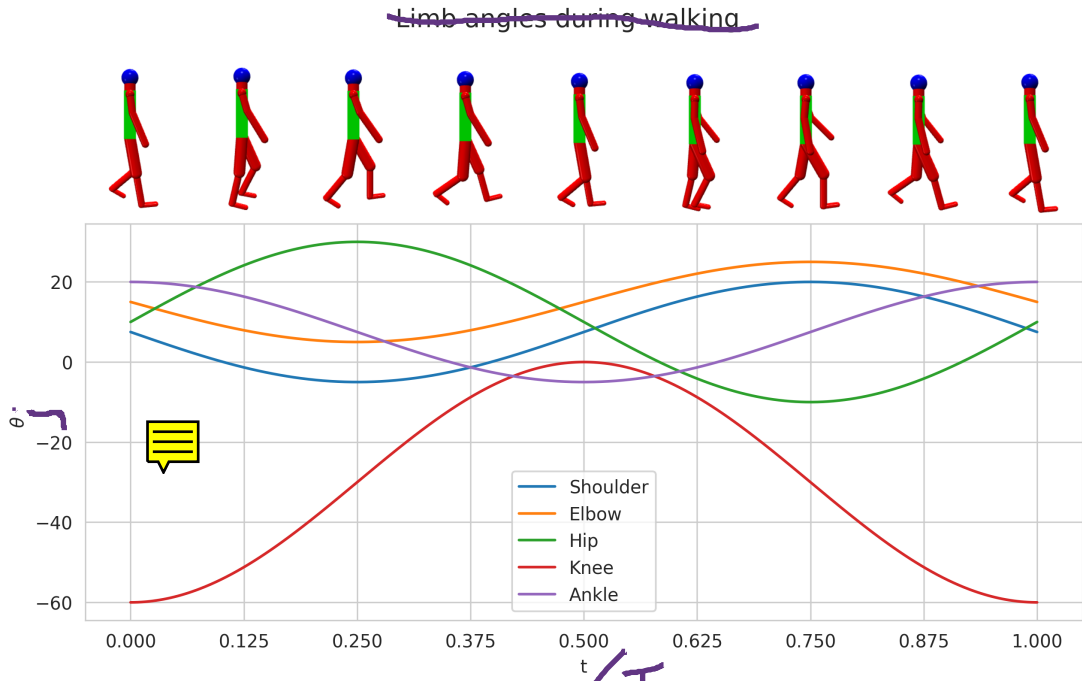


Figure 5: Graph of the angles θ of the various limbs during walking over period $T = 1$, with a visualization of our model as reference.

- During walking the torso is straight, while during running it forms a constant angle with the z axis of 8° [13].

A plot of the angles θ over a period $T = 1$ can be seen on Fig. 5 for walking and on Fig. 6 for running, both complete with a visualization of the model during a period. As with the base body, the numerical details of both our walking and running bodies can be found on GitHub at <https://github.com/Cr3sp1/RainSimulation/tree/main/Bodies>.

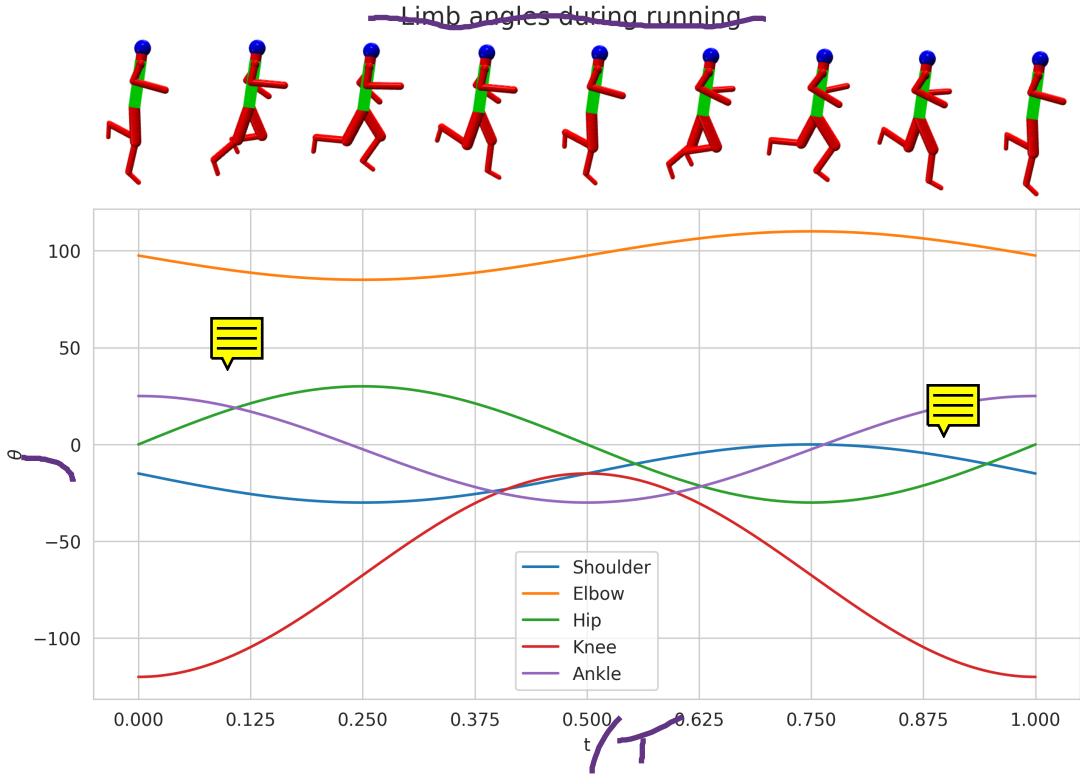


Figure 6: Graph of the angles θ of the \square as limbs during running over the period $T = 1$, with a visualization of our model as reference.

3 Technical implementation

WIP: here will be a description of the code. We call dx the distance between our generated ray origins.

3.1 Code validation

We proceed to check that our code works properly. To do so we compare the numerical results we \square for \square sphere, parallelepiped and capsule with the analytic results obtained in Sec. 2. We call $\tilde{R}_b(dx)$ the \square of R_b evaluated with our code with a step dx . The error $\Delta R_b(dx)$ then is the difference $\square \tilde{R}_b(dx)$ and $\square R_b$ evaluated analytically:

$$\Delta R_b(dx) = \tilde{R}_b(dx) - R_b. \quad (25)$$

The absolute error is then $|\Delta R_b(dx)|$. We assume that the absolute error follows a power law:

$$|\Delta R_b(dx)| = \alpha(dx)^\beta, \quad (26)$$

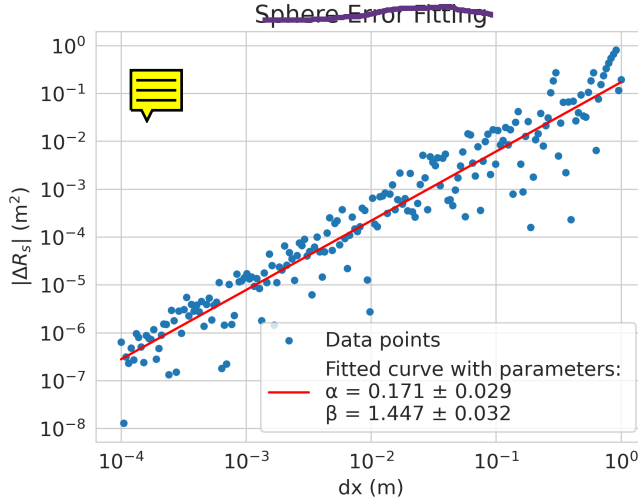


Figure 7: Fit with a power law of the error on R_s of a sphere.

where α and β are parameters to determine. We check that this is the case. With a set body, \mathbf{v}_r and v_b we evaluate ΔR_b for 200 different dx values ranging from 0.0001 m to 1 m. We then fit the data to the power law. To do so we first take the logarithm on both sides of Eq. (26):

$$\ln(|\Delta R_b(dx)|) = \ln(\alpha) + \beta \ln(dx). \quad (27)$$

We then evaluate α and β with a least squares regression. We use the same \mathbf{v}_r and v_b for each body to better be able to compare the results. The following results are for $v_{tail} = 0.5 v_{fall}$, $v_{cross} = 0.25 v_{fall}$ and $v_{tail} = 2 v_{fall}$. As solids consider a sphere with radius $r = 0.5$ m, a parallelepiped with sides $\mathbf{s}_1 = (0.4, 0, 0)$ m, $\mathbf{s}_2 = (0, 0.6, 0)$ m, $\mathbf{s}_3 = (0, 0, 0.8)$ m, and a capsule with a radius $r = 0.3$ m and $\Delta \mathbf{l} = (0.4, 0.4, 0.4)$ m. We can see the results for the sphere on Fig. 7, for the parallelepiped on Fig. 8 and for the capsule on Fig. 9. In all these cases we can see the power law described by equation (26) provides a good fit for $|\Delta R_b(dx)|$. The most important difference is in the value of β : for the parallelepiped we found $\beta = 1.062$ compared to $\beta = 1.447$ and $\beta = 1.537$ for the sphere and capsule respectively. This slower convergence of $\tilde{R}_p(dx)$ to R_p could be due to the more complex shape of the projection of the parallelepiped, with sharp edges and vertices.

In Fig. 10, 11 and 12 we see a comparison of $R_b(v_b)$ and $\tilde{R}_b(v_b, dx)$ for a varying v_b with the same solids and parameters before and $dx = 0.001$ m, which in this case provides a precision sufficient to determine the existence of minimum in $R_b(v_b)$. These graphs also provide a good example of a case in which the shape of the body determines the existence and value of an ideal speed.

Another aspect of the code we check is its ability to handle simple base bodies correctly. To do so we consider a complex body composed by two parallelograms: p_1

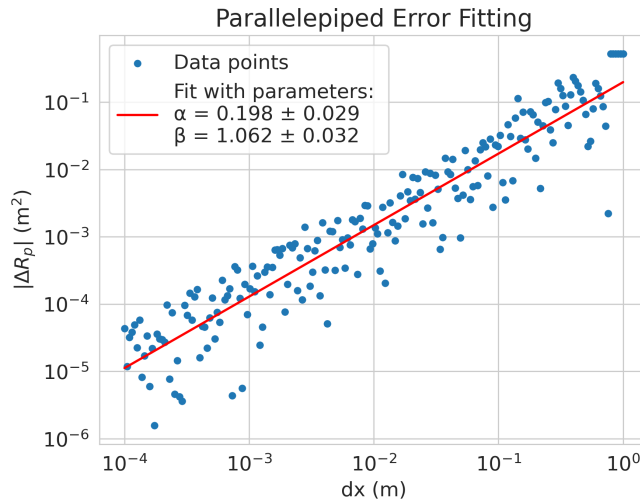


Figure 8: Fit with a power law of the error on R_p of a parallelepiped.

with sides $(0.8, 0, 0)$ m, $(0, 0.5, 0)$ m and $(0, 0, 0.8)$ m, and p_2 with sides $(0.6, 0, 0)$ m, $(0, 0.3, 0)$ m and $(0, 0, 0.6)$ m. We call \mathbf{c}_1 the center of p_1 , and \mathbf{c}_2 the center of p_2 . We consider $v_b = v_{fall}$, and $v_{tail} = v_{cross} = 0$. We then evaluate the ratio R_{2p} as we move \mathbf{c}_2 along the y axis starting from $\mathbf{c}_2 = \mathbf{c}_1$. We expect that at the start p_2 is contained inside p_1 , so $R_{2p} = R_{p2}$, but as $|\mathbf{c}_2 - \mathbf{c}_1|$ increases we expect R_{2p} to remain constant while p_2 remains fully inside p_1 , then increase as p_2 gradually comes out, and finally remain constant again as p_2 is fully outside. Furthermore since v_{rel} has no y component, p_1 and p_2 do not overshadow one another as long as they are no longer in contact, so we expect the final value of R_{2p} to simply be $R_{p1} + R_{p2}$. You can see in Fig. 13 that R_{2p} behaves exactly as described.

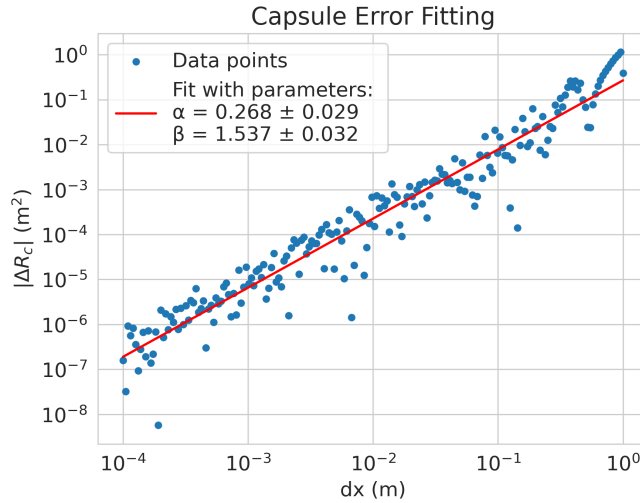


Figure 9: Fit with a power law of the error on R_c of a capsule.

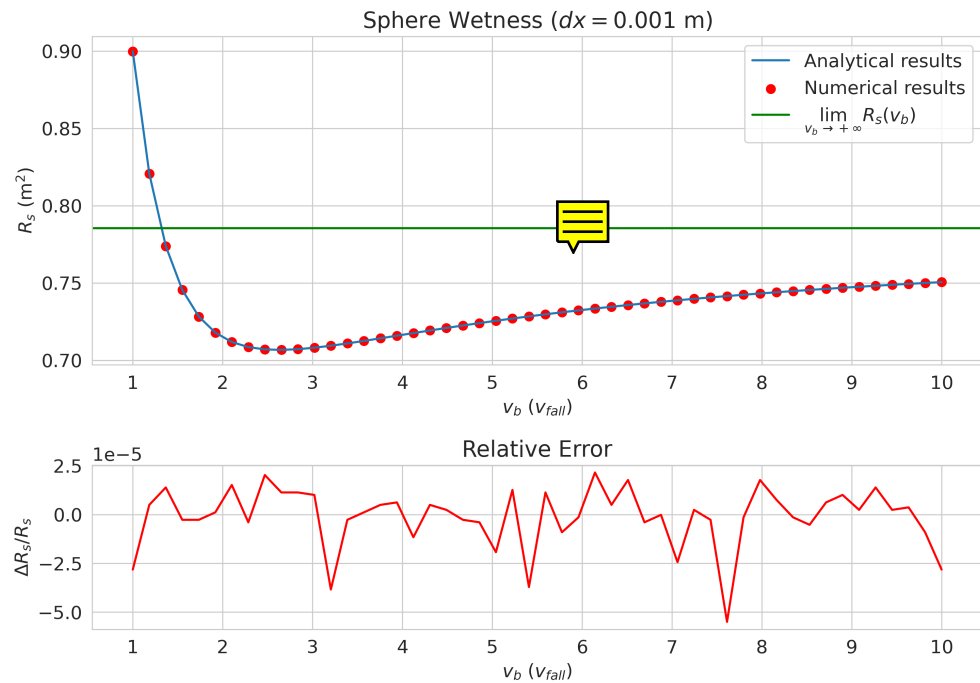


Figure 10: Graph of $R_s(v_b)$ and $\tilde{R}_s(v_b, dx)$ of a sphere for a variable v_b and a fixed $dx = 0.001 \text{ m}$.

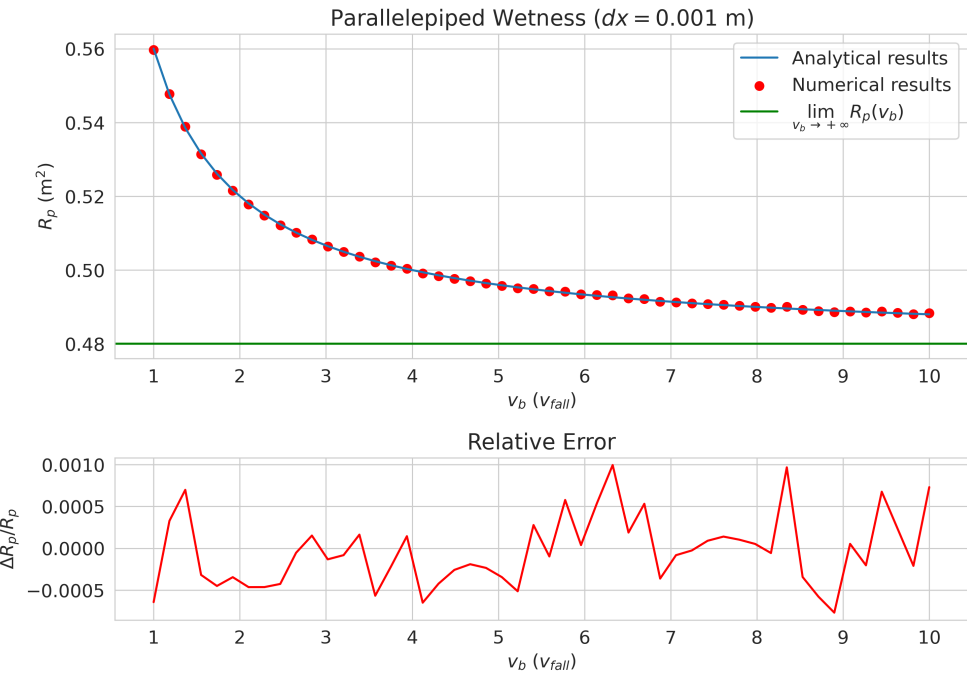


Figure 11: Graph of $R_p(v_b)$ and $\tilde{R}_p(v_b, dx)$ of a parallelepiped for a variable v_b and a fixed $dx = 0.001$ m.

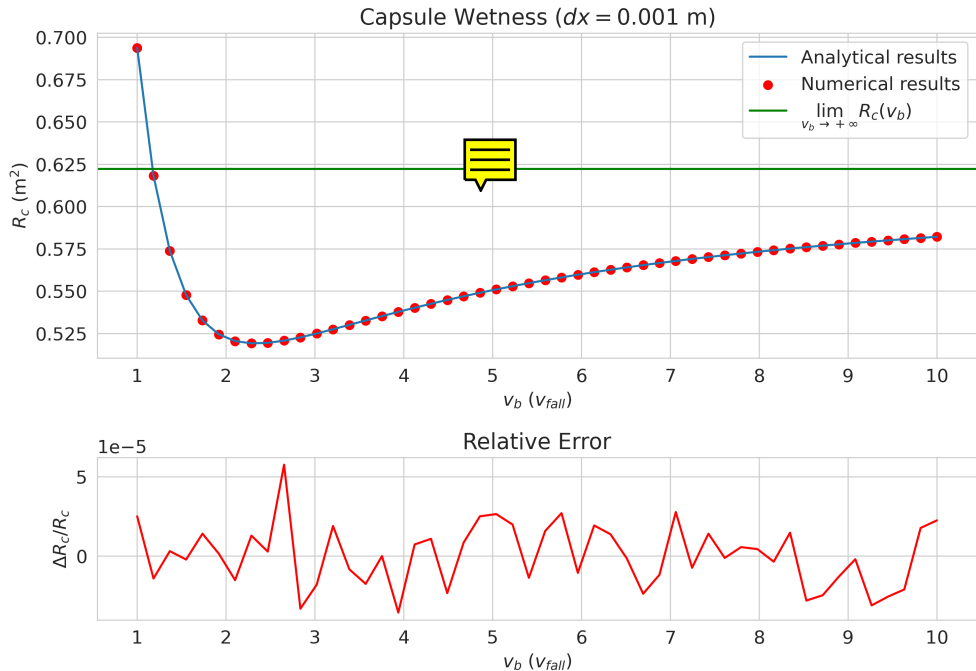


Figure 12: Graph of $R_c(v_b)$ and $\tilde{R}_c(v_b, dx)$ of a capsule for a variable v_b and a fixed $dx = 0.001$ m.

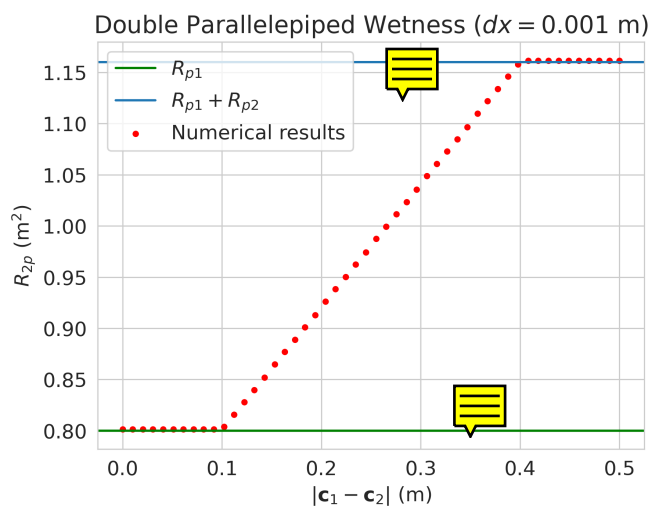


Figure 13: Graph of R_{2p} of two parallelepipeds as the distance between their centers increases.

4 Results

5 Discussion and Conclusion

References

- [1] B. L. Schwartz, M. A. B. Deakin, Math. Mag. **46**, 272 (1973).
- [2] D. Hailman, B. Torrents, Math. Mag. **82:4**, 266 (2009).
- [3] F. Bocci, Eur. J. Phys. **33**, 1321 (2012).
- [4] T. Kroetz, Rev. Bras. Ensino Fis. **31:4**, 4304 (2009).
- [5] L. Pournin, M. Weber, M. Tsukahara, J. A. Ferrez, M. Ramaioli, T. M. Liebling, Granular Matter **7**, 119 (2005).
- [6] D. C. Lay, S. R. Lay, J. J. McDonald, *Linear algebra and its applications*, 5th ed. (Pearson Education, 2014).
- [7] R. Schneider, *Convex bodies: the Brunn–Minkowski theory* (Cambridge Univ. Press, 1993).
- [8] P. Huang, S. Pan, Y. Yang, Discrete Comput. Geom. **54**, 728 (2015).
- [9] L. da Vinci, *Uomo vitruviano* (1490). 
- [10] A. K. Yegian, Y. Tucker, S. Gillinov, D. E. Lieberman, J. Exp. Biol. **220**, 13 (2019).
- [11] T. J. van der Zee , E. M. Mundinger, A. D. Kuo1, Sci Data **9**, 704 (2022).
- [12] P. R. Cavanagh, Foot Ankle **7**, 197 (1987).
- [13] A. F. dos Santos, T. H. Nakagawa, G. Y. Nakashima, C. D. Maciel, F. Serrão, Int. J. Sports. Med. **37**, 369 (2016). 